Materials & Design 247 (2024) 113369

Contents lists available at ScienceDirect

Materials & Design

journal homepage: www.elsevier.com/locate/matdes

Biophotonic composite scaffolds for controlled nitric oxide release upon NIR excitation

S. Ghanavati [a,b,*], E. Santos Magalhaes [b], C. Nguyen [b], B. Bondzior [b,c], M. Lastusaari [d], J.N. Anker [e], A. Draganski [f], L. Petit [b,*], J. Massera [a]

[a] Faculty of Medicine and Health Technology, Tampere University, Korkeakoulunkatu 3, Tampere 33720, Finland
[b] Photonics Laboratory, Tampere University, Korkeakoulunkatu 3, Tampere 33720, Finland
[c] Institute of Low Temperature and Structure Research PAS, Okolna 2, 50-422, Wrocław, Poland
[d] Department of Chemistry, University of Turku, FI-20014 Turku, Finland
[e] Departments of Chemistry and Bioengineering, Clemson University, Clemson, SC, USA
[f] Zylö Therapeutics, Greenville, SC, USA

ARTICLE INFO

Keywords:
Bioactive glass
Porous scaffold
$CaWO_4$ crystals
Upconversion

ABSTRACT

For the first time, the preparation of 3D biophotonic scaffolds is reported. Scaffolds are prepared using the porogen burn-off technique and are capable of converting NIR to green emission, used to release nitric oxide from S-Nitroso-N-Acetylpenicillamine. NIR to green conversion is obtained by mixing $CaWO_4$ crystals (codoped with Yb^{3+} and Er^{3+}) with bioactive borosilicate glass prior to the sintering process. The scaffold fabrication process has a detrimental impact on the upconversion properties of the crystals embedded in the porous scaffold due to the formation of internal/surface crystalline defects and surface chemical bonds in the crystals. Nonetheless, we demonstrate that the brightness of the green emission, under 980 nm pumping, is sufficient to release nitric oxide from the scaffold covered with S-Nitroso-N-Acetylpenicillamine. Addition of upconverter crystals, in the bioactive scaffold, has no impact on porosity, mechanical properties, reactivity in simulated body fluid nor cytocompatibility. The progressive dissolution of the scaffold, associated with the precipitation of a reactive layer (HA), has no noticeable influence on the green emission under 980 nm pumping, showing that the development of such biophotonic scaffolds opens the path to light actuated drug release in a spatial–temporal manner, in vivo. Degradation of the up-converter particles does not lead to differences in cells viability.

1. Introduction

Glasses are promising materials for various applications as their composition can be easily tailored [1]. While traditional glasses, used in cookware, lighting, optical fibers etc. are known for their hydrolytic resistance, L.L. Hench developed, in 1969, the first resorbable glass able to promote bone regeneration [2]. Since this groundbreaking discovery, and pertaining to the versatility of glasses, many compositions have been developed for application in bone tissue engineering [3]. However, despite the tremendous effort from the scientific community, only few compositions have been translated to clinics, such as 45S5, S53P4 and 13–93 [2,4,5]. Recently, a borosilicate glass, with the composition $26.93SiO_2 – 26.93B_2O_3 – 22.66Na_2O – 1.72P_2O_5 – 21.77CaO$ (in mol%), was developed and was reported to be a good candidate for bone graft pertaining to its ability to overexpress osteocalcin and osteopontin, signs of osteogenic commitment, when culturing human adipose stem cells [6]. The presence of boron, in the structure, was found to strongly enhance the expression of vWF and PECAM-1, markers of the angiogenesis [7]. The good thermal stability, against crystallization, of this glass, enabled the preparation of 3D porous scaffolds using a robocasting 3D extrusion printing process followed by sintering. Post-sintering, the scaffolds were amorphous and maintained their ability to produce hydroxyapatite, upon immersion in physiological medium [8].

This 3D porous structure is of great interest as the surface can act as a template for cell attachment and promoting cell proliferation. The porosity also affects all aspects of bone physiology including diffusion and transport of nutrients, cells, and ions, in turn driving the osteogenic and angiogenic properties of the medical device. The possibility of using

* Corresponding authors at: Faculty of Medicine and Health Technology, Tampere University, Korkeakoulunkatu 3, Tampere 33720, Finland. (J. Massera) (S. Ghanavati) / Photonics Laboratory, Tampere University, Korkeakoulunkatu 3, Tampere 33720, Finland. (S. Ghanavati).
E-mail addresses: sonya.ghanavati@tuni.fi (S. Ghanavati), jonathan.massera@tuni.fi (L. Petit).

https://doi.org/10.1016/j.matdes.2024.113369
Received 2 May 2024; Received in revised form 8 October 2024; Accepted 8 October 2024
Available online 10 October 2024

such 3D porous materials for localized drug delivery has gained interest, especially since the report published by the European Center for Disease Prevention and Control (ECDC) and the World Health Organization (WHO) Europe Regional Office, calling for greater effort in effectively tackling antimicrobial resistance [9]. Antimicrobial resistance is exacerbated in implant related infections and therefore should attract more attention from scientists. Soundrapandian et al reported a study on a new bioactive porous scaffold, prepared using porogen burn-off technique, that could deliver drugs for 6 weeks in vitro [8]. In their study, the scaffolds were loaded with gatifloxacin prior to implantation so there was no control over the drug release rate or overall dose over time. Thus, bioactive biomaterial (possessing osteogenic and angiogenic properties) prepared, with an actuator, able to specifically release an active agent upon a specific stimulus would be of great interest.

As an external stimulus, light is a powerful tool for triggering chemical reactions in biological environment with rapidity and accuracy without affecting important physiological parameters such as temperature, pH, and ionic strength. Phototriggered release mechanisms are particularly promising because the illumination time, spot size, wavelength and dose can easily be controlled. Successful release of nitric oxide (NO) using light has been reported [10]. NO is a bioregulatory free radical molecule and has various functions in the body such as controlling vasodilation of blood vessels or acting as a neurotransmitter, for example [11]. S-nitroso-N-acetyl-D-penicillamine (SNAP) has been intensively investigated for NO release which was found to be effective antimicrobial agents [11,12]. Recently, Hopkins et al demonstrated the controlled release of NO using light emitting diodes (LEDs) at 460 nm [10]. The use of the LEDs at 460 nm has a major limitation as light at 460 nm is strongly attenuated in tissue preventing therapeutic effect in deep tissue while strongly affecting overlying tissue [13]. These problems can be mitigated using upconverter phosphors. These phosphors can convert in-situ the deep tissue penetrating near-infrared light into visible useful in the phototriggered release of NO for example.

Crystal are promising upconverting materials, especially when designed with a low phonon energy as the rate of nonradiative multiphonon relaxation from upper levels is reduced enhancing the efficiency of the up-conversion process [14]. Ye and co-workers demonstrated that $NaYF_4$ crystals doped with Yb^{3+} and Nd^{3+} can be used to convert 808 nm light into UV/blue light to release NO from *N,N′*-Di-*sec*-butyl-*N,N′*-dinitroso-1,4-phenylenediamine [15]. Li and co-workers reported the fabrication of 3D printed bone scaffold with $Ca_{19}Zn_2(PO_4)_{14}$ crystals doped with Yb^{3+} and Ho^{3+} and emitting green light under 980nm excitation not only for anti-infection application but also for tracking the scaffold degradation in vivo [16]. $CaWO_4$ is another promising host for RE ions due its low phonon threshold energy [17]. $CaWO_4$ has a tetragonal structure with distorted $[WO_6]$ octahedral clusters [18] and can be co-doped with Yb^{3+} and Er^{3+} even if no trivalent cation positions exist [19]. The Er^{3+} and Yb^{3+} cooping can also be used to convert 980nm into green light [14]. Indeed, Yb^{3+} ions absorb 980 nm light and transition to the excited $^2F_{5/2}$ state, from which the energy is transferred to Er^{3+} ions leading to higher energy photon emissions after two-photon pile-up.

In this paper, we demonstrate for the first time to the best of our knowledge, the NO release from bioactive porous scaffolds able to emit green light upon excitation at 980 nm which is commonly applied to tissue including in photodynamic therapy and sensing [20]. We report the use of the porogen burn-off technique to prepare such porous scaffold. The upconversion properties are achieved by adding Yb^{3+}, Er^{3+}: $CaWO_4$ crystals in the glass powder prior to the sintering process. The crystal mass fraction in the glass needs to be high enough for bright upconversion emission while still processing a porous scaffold with target porosity (at least 60%) and mechanical properties (at least in the range of the cancellous bone) [21]. We demonstrate that the green light from the scaffold is strong enough to trigger NO release from SNAP containing scaffolds and that the addition of the crystals has no impact on the scaffold response when immersed in simulated body fluid (SBF). The current formulation was designed to show proof-of-principle and has not been optimized for long term in vivo storage and release. However, other groups have demonstrate that SNAP can be retained over months with proper selection of polymer or covalent linkage. For example, Brisbois and co-workers demonstrate retention of 82% of after 2 months at 37 °C [22] and Hopkins et al show sufficient release for antimicrobial inhibition up to at least 125 days [23].

2. Materials and Methods

The $26.93SiO_2 – 26.93B_2O_3 – 22.66Na_2O – 1.72P_2O_5 – 21.77CaO$ (in mol%) glass was prepared using standard melt quenching process. The raw materials were SiO_2 (Umicore, 99.99%), H_3BO_3 (Sigma Aldrich, >99.5%), Na_2CO_3 (Honeywell, >99.5%), $CaCO_3$ (AlfaAesar, 99%), and $CaHPO_4{\cdot}2H_2O$ (Sigma Aldrich, >99.5%). The 30 g glass batch was melted at 1250 °C for 1 h. After quenching, the glass was annealed at 40 °C below its glass transition temperature. Finally, to ease flow sintering and densification, the annealed glass was crushed and sieved to a particle size of <38 μm as in [24].

Solid state-reaction was used to prepare the $CaWO_4$ crystals as in [25]. As in [26], Na^+ was used to compensate charge when doping the crystals with Yb^{3+} and Er^{3+} at the expense of Ca^{2+}. $CaCO_3$ (Alfa-Aesar, technical grade), WO_3 (Honeywell-Fluka, 99%), Yb_2O_3 (Sigma-Aldrich, 99.9%), Er_2O_3(Sigma-Aldrich, 99.9%) and Na_2CO_3 (Sigma-Aldrich, 99.9%) were heated to 1200 °C in air for 4 h. The concentration of Yb was 15 at % whereas the concentration of Er ranged from 0.25 to 0.75 at %. The crystals are labeled as 15Yb – xEr, where x is the Er concentration. Similarly to [26], the crystals have various shapes and sizes (between ~10 μm and 30 μm), independently of the rare-earth concentration.

The scaffolds were prepared using the porogen burn-off technique as described in [24]. The glass particles were mixed with different amounts of $CaWO_4$ crystals, from 0 to 15 wt%, prior to being mixed with the porogen NH_4HCO_3 (Sigma Aldrich, >99.5%) with a glass-crystal to porogen ratio of 30/70 in volume. The mixture was then pressed into pellets at 25 MPa and heat-treated at 300 °C for 5 h, for the porogen to decompose and evaporate, and finally sintered at 555 °C for 1h.

Simulated body fluid (SBF) (refined SBF protocol as proposed in [27]) with a pH of 7.4 at 37 °C (±0.2 °C) was used for the in-vitro testing. The scaffolds prepared with 10 wt% of the 15Yb – 0.75Er $CaWO_4$ crystals were immersed in SBF for up to 2 weeks in an incubating shaker (120 RPM). The SBF volume to mass of scaffold ratio was 10mg/ml. For ICP-OES (ICP-OES 5110, Agilent technology, USA) analysis, 1 ml of the immersed solution was diluted in 9 ml of 1M HNO_3.

The scaffolds prepared with 10 wt% of the 15Yb – 0.75Er $CaWO_4$ crystals were covered with S-Nitroso-N-Acetylpenicillamine (SNAP) which was made by dissolving 50 mg of Penicillamine into 1 ml of dimethyl sulfoxide (DMSO) (50 mg/mL) followed by equimolar addition of sodium nitrite (100 μL of 1 M solution) and hydrochloric acid (100 μL of 1 M solution). After thorough vortex mixing, this solution was incubated at room temperature for 1 h. The color of the solution turned deep green indicative of formation of the nitrosation product SNAP. The complete conversion of penicillamine to SNAP was confirmed by UV–Vis absorption using an extinction coefficient of 0.7 $(mg/mL)^{-1}$ cm^{-1}. A total of 500 μL of the SNAP solution was added to the dry scaffold so that all surfaces of the scaffold had a dark green color. Brightfield microscopy (10x objective) was used to confirm that SNAP was evenly deposited across the scaffold surfaces. A 980 nm 0.5 W laser (MIL-III-980-500mW) was used to irradiate the SNAP functionalized scaffold. The NO Analyzer (Eco Physics, CLD 60) was used to quantify the release of NO.

The upconversion (UC) spectra of the crystals and scaffolds were measured using a TEC-cooled fiber-coupled multimode laser (II-VI Laser enterprise) at λ_{exc} = 980 nm and the Spectro 320 optical spectrum analyzer (Instrument Systems Optische Messtechnik GmbH, Germany). The absolute upconversion intensity was recorded with a Hagner ERP-105 photometer using the SD27 photopic luminance detector from

emission induced by a Thorlabs MCLS1-980-20 980 nm laser (15 mW) at full power. Both the excitation and the detector were placed 5 mm away from the sample surface. The measurements were obtained at room temperature and from sample crushed into powder to allow the comparison of the emission intensity.

The mechanical properties of the dried scaffolds (Young's modulus and fracture strengths) were tested in compression, using an Instron Electropuls®, E1000. Values were extracted from the load–displacement curve and are reported as mean ± SD (n=5).

Live/Dead assay was used to investigate scaffolds cytotoxicity in direct contact with human adipose stem cells (hADSCs). Prior to the cell test, scaffolds were pre-incubated for 1 day in 2 ml of αMEM (1% P/S). The density of hADSCs used for seeding was 1,100 cells/cm^2 in 1 ml of α-MEM culture medium and cultured in direct contact with the scaffolds in static condition. The culture medium was changed after 44 and 144 h. At 1-, 3- and 7-days, the samples were rinsed with Dulbecco's Phosphate Buffered Saline, DPBS (Gibco, Life Technologies, Carlsbad, CA, USA) and incubated with staining solution, prepared according to the Live & Dead Kit (Invitrogen, Life Technologies, Carlsbad, CA, USA), for 30 min at room temperature. Viable and necrotic hADSCs were stained with 1 % (v/v) of Calcein AM and 0.5 % (v/v) Ethidium Homodimer-1 solution. Finally, the samples were rinsed and observed under the fluorescence microscope (Olympus IX51).

3. Results and discussion

In order to prepare a scaffold which emits green light under 980 nm pumping, $CaWO_4$ crystals were synthesized using solid-state reaction as in [14,18,28] and were doped with Yb^{3+} and Er^{3+}. Compared to [29], the amount of Yb and Er introduced in the crystals are larger in order to prepare crystals with intense green light under 980 nm pumping. As shown in Fig. 1**a**, the X-ray diffraction pattern of the crystals, with fixed Yb content at 15 at%, did not depend on Er concentrations (0.25–0.75 at %).

The peaks matched the standard Powder Diffraction File entry 04-008-6874 of $CaWO_4$ crystalline phase. The sharp XRD peaks indicate that the samples are well crystallized, in agreement with our previous work focused on $CaWO_4$ co-doped with Yb^{3+} and Tm^{3+} [26]. Under 980 nm pumping, the crystals exhibit emissions at 525 and 550 nm which can be related to the $^2H_{11/2}$, $^4S_{3/2} \rightarrow {}^4I_{15/2}$. The upconversion spectrum also depicts a band at 650 nm which can be assigned to the $^4F_{9/2} \rightarrow {}^4I_{15/2}$ transitions of Er^{3+} (Fig. 1**b**). As the Er^{3+} at % increases, the intensity of the green and red emissions increases showing that the concentration of Er ions in the $CaWO_4$ crystals can be as high as 0.75 at% without concentration-quenching effect (Fig. 1**c**). It is well known that the UC emission intensity (I) is proportional to P^n, P being the excitation power and "n" the number of pump photons absorbed per UC photon emitted. At very low powers, an I^2 dependency is expected for a 2-photon process (a slope of 2 on a log–log scale), but as power increases, excitation saturation effects gradually reduce this slope. As depicted in Fig. 1**d**, the slopes of the emissions at 525, 550 and 650 nm are 1.90, 1.74, and 1.65 respectively indicating that the upconversion emissions are due to two-photon processes with moderate saturation. Similar slopes were reported for $CaWO_4$ codoped with 5 at% Yb^{3+} and 0.3 at%Er^{3+} [19]. The 980 nm pump excites the Er^{3+} ions to the $^4I_{11/2}$ level due to the transition from the ground state but also from the energy transfer (ET) from Yb^{3+} which is the most probable excitation route due to the high absorption cross-section of Yb^{3+} ions. The $^4F_{7/2}$ level is then populated from the $^4I_{11/2}$ level from the excited state absorption process ($^4I_{11/2} + h\nu \rightarrow {}^4F_{7/2}$) and from the dominant energy transfer process ($^4I_{11/2}$ (Er^{3+}) + $^2F_{5/2}$ (Yb^{3+}) $\rightarrow {}^4F_{7/2}$ (Er^{3+})+ $^2F_{7/2}$ (Yb^{3+})). Finally, there is a non-radiative transition from the $^4F_{7/2}$ level to the $^2H_{11/2}$ and $^4S_{3/2}$ levels

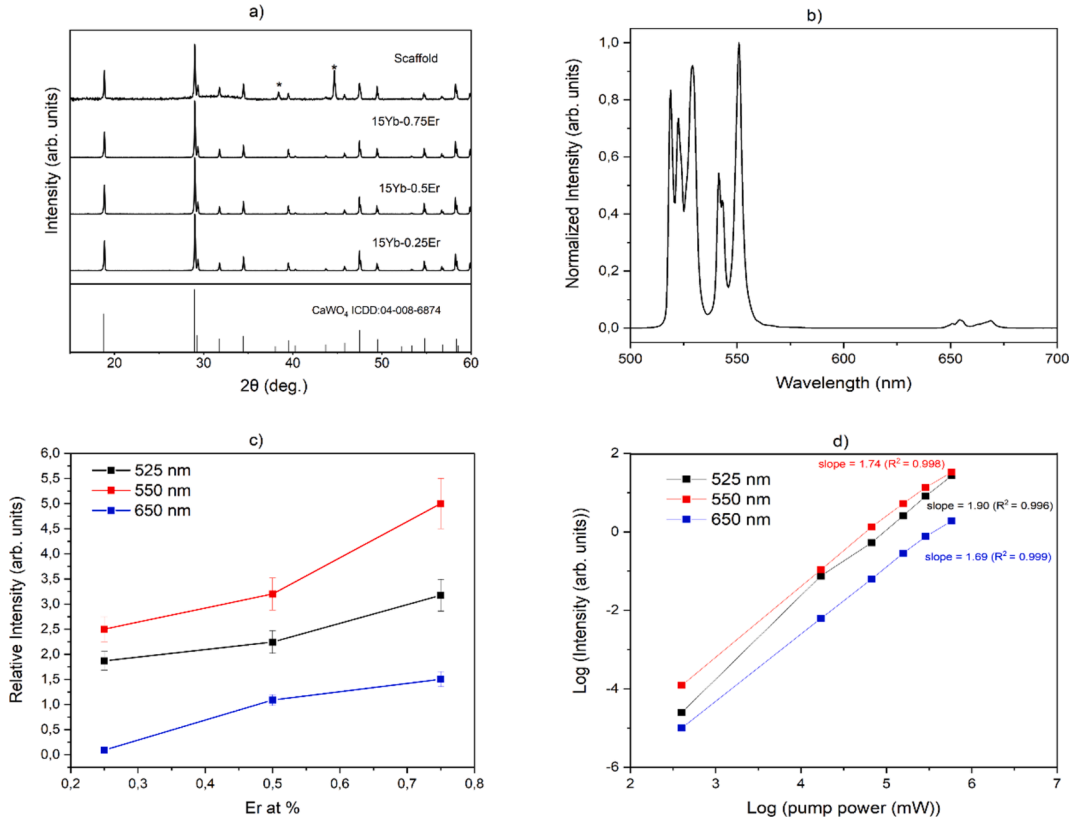

Fig. 1. XRD pattern of the $CaWO_4$ crystals codoped with 15 at% of Yb and 0.25–0.50–0.75 at % of Er and of the composite scaffold prepared with 10 wt% of the 15Yb – 0.75Er crystals, taken as an example (a), Upconversion spectra of the 15Yb – 0.75Er crystal, taken as an example, obtained under 980 nm pumping (b), Relative intensity of the green and red emissions as a function of Er at % (c) and dependence of the emission intensity at 525, 550 and 650 nm on the excitation power density for the 15Yb – 0.75Er crystal, taken as an example The numbers labeling the curves are the slopes on a log–log scale, which represent a power-law dependency (d).

from which there is a radiative transition to the Er^{3+} ground state leading to green emissions centered at 525 and 550nm, respectively. As a result of a non-radiative relaxation from $^4I_{11/2}$ to $^4I_{13/2}$ in Er^{3+}, the energy transfer $^4I_{13/2}$ (Er^{3+}) + $^2F_{5/2}$ (Yb^{3+}) → $^4F_{9/2}$ (Er^{3+}) + $^2F_{7/2}$ (Yb^{3+}) also occurs leading to red emission due to the radiative transition from the $^4F_{9/2}$ (Er^{3+}) to the Er^{3+} ground state. Red emission can also be due to cross-relaxation process: $^4I_{13/2}$ (Er^{3+}) + $^4I_{11/2}$ (Er^{3+}) → $^4F_{9/2}$ (Er^{3+}) + $^4I_{15/2}$ (Er^{3+}). The absolute photopic range (ca. 490–630 nm) upconversion emission intensity of the 15Yb – 0.75Er crystal was measured at 24.40 cd/m^2 under ca. 3 W/cm^2 power density using 980 nm laser diode, which is smaller than the brightness reported for $(Y_{0.85}Yb_{0.10}Er_{0.05})_2O_3$ crystals (169.4cd/m^2 under 5.56W/cm^2 980 nm pump density), for example [30]. However, one should be careful when comparing brightness of crystals as the brightness measurement is not entirely straightforward and depends on incident power density. Nonetheless, one can mention that the newly developed crystals emit green light which can be seen by naked eye which has the standard limit of light perception at 0.32×10^{-5} cd/m^2 [30].

Composite scaffolds were prepared using the porogen burn-off technique by sintering the glass with the 15Yb – 0.75Er crystals. All the scaffolds, independently of the amount of the crystals, exhibit a porosity of (68 ± 2.5) % (measured as in [31]) which is well in line with the reported optimal porosity required for bone application (>60% porosity). The XRD pattern of the biophotonic scaffold exhibits XRD peaks which can be related to the $CaWO_4$ crystalline phase but also 2 additional peaks (*) with low intensity. Since no crystallization was reported to occur in this glass during sintering process [32], the presence of additional peaks in the XRD pattern suggests that the addition of crystals in the glass powder leads to the precipitation of an additional crystalline phases in the glass matrix during the sintering process (Fig. 1**a**). However, the number of peaks is too small to allow the identification of the crystalline phase. These peaks could be related to the $CaNa_3B_5O_{10}$ crystalline phase which was found to precipitate in this glass during thermal treatment at higher temperature than the sintering temperature [32]. Despite the presence of this second crystalline phase, all scaffolds emit, under 980 nm pumping, green light, the intensity of which increases as expected with an increase in the up-converter crystal wt% in the scaffold (Fig. 2**a**).

The mechanical properties of the scaffolds prepared with various wt % of crystals were measured and are reported in Table 1.

Overall, the addition of luminescent crystals does not affect the mechanical properties of the scaffolds. All scaffolds exhibit a compressive strength at around 1 MPa and Young's modulus at around 30 MPa, independently of the amount of crystals. These scaffolds, produced by the burn-off technique, have similar mechanical properties than those than reported for thermally bonded bioactive glass particles [33]. Those mechanical properties fall within the lower range of the mechanical properties of trabecular bone. While the mechanical properties are low, it should be pointed out that the scope, here, was to develop luminescent scaffold with mechanical properties enabling their handling. Despite their Young's modulus of (37 ± 15 MPa), the scaffolds prepared with 15 wt% of crystals were fragile and tended to break easily. Therefore, based on the emission and mechanical properties, the scaffolds prepared with 10 wt% of $CaWO_4$ crystals were selected for further investigation.

Table 1
Fracture strength and Young's modulus of the sintered scaffolds produced by the porogen burn-off technique, as a function of crystals loading.

	Fracture strength, MPa	Young's modulus, MPa
2.5 wt%	1.07 ± 0.35	33 ± 14
5 wt%	1.02 ± 0.38	25 ± 18
7.5 wt%	0.95 ± 0.25	35 ± 15
10 wt%	0.94 ± 0.37	40 ± 14
15 wt%	0.91 ± 0.40	37 ± 15

Although the 15Yb – 0.75Er crystals survive the sintering process, the scaffold fabrication process has an impact on the UC properties: the intensity of the green and red emission decreases (Fig. 2**b**) and the power dependence slopes of the emissions at 525, 550 and 650 nm decreases after pressing and sintering the mixture composed of the porogen, glass and the 15Yb – 0.75Er crystals (Table 2). These changes suggest that the scaffold fabrication has an impact on the site of the rare-earth ions. As reported in [34,35], the thermal treatment and/or the pressing step could lead to internal/surface crystalline defects and surface chemical bonds with detrimental impact on the UC properties of the crystals.

An absolute intensity of 2.23cd/m^2 under 3 W/cm^2 power density using 980 nm laser diode was measured from the most promising scaffolds prepared with 10 wt% of crystals. This brightness level was found to be enough to release NO from the SNAP functionalized scaffolds (Fig. 3**)**.

Table 2
Slope of the dependence of the intensity of the emissions at 525, 550 and 650 nm on the excitation power density.

	Slope of the dependence on the excitation power density of the intensity of the emissions at		
	525 nm	**550 nm**	**650 nm**
As-prepared crystals	1.90	1.74	1.69
Pressed glass, porogen and crystals mixture	1.94	1.52	1.60
As-prepared scaffold	1.92	1.30	1.57

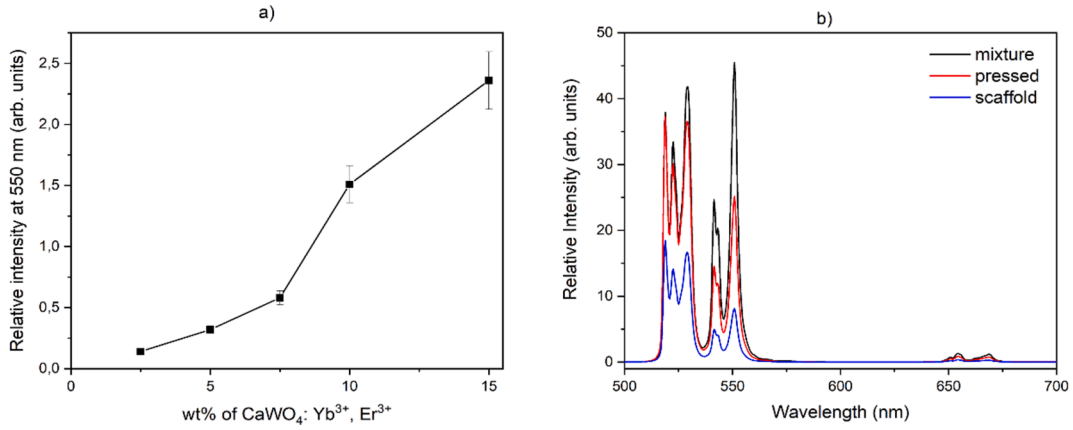

Fig. 2. Intensity of the emission at 550 nm of the scaffolds prepared with different wt% of the 15Yb – 0.75Er $CaWO_4$ crystals (a) and upconversion spectra of the mixture of glass, porogen and 10 wt% of the 15Yb – 0.75Er $CaWO_4$ crystals, prior to and after pressing (pressed) and sintered into scaffold (scaffold) (b). The upconversion spectra are obtained using 980 nm pumping.

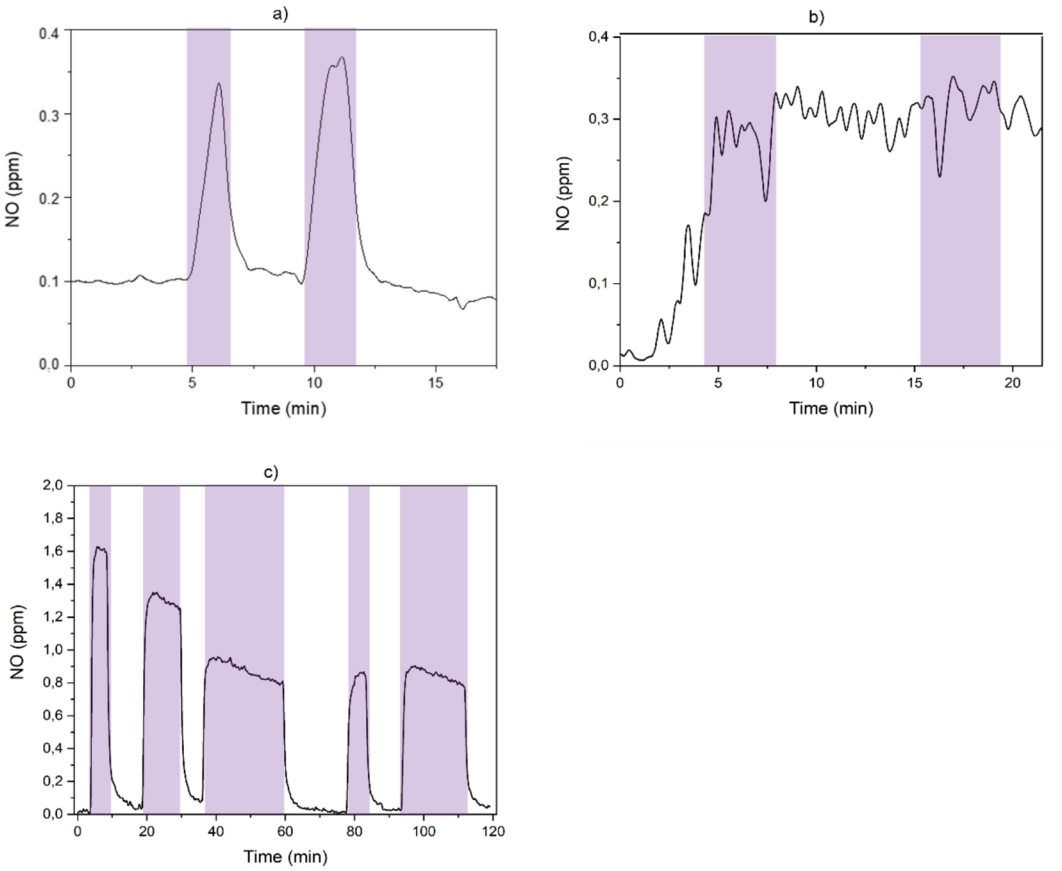

Fig. 3. 980 nm light modulate NO release from upconverter (a) and undoped (b) scaffolds coated with nitric-oxide releasing SNAP. White light modulated NO release from undoped scaffold coated with nitric-oxide releasing SNAP after waiting 3 days to remove initial burst release background (c). The color indicates when the 980 nm laser and white light are on.

As a proof of concept, the SNAP functionalized scaffolds were irradiated with 980 nm. As seen in Fig. 3**a**, the brightness level produced by the upconverter crystals efficiently photocleave the NO from the SNAP. NO release stopped once the excitation was stopped confirming optimum control over the NO release using light stimulus. Modulation of the NO release from the upconverter crystals was further proven by the lack of NO release under 980 nm excitation from scaffold prepared without $CaWO_4$ crystals (Fig. 3**b**). Effect of light intensity on NO release kinetics is under progress and will be published separately.

Effort was focused on effect of light wavelength on NO release kinetics. White light modulated NO release from undoped scaffold coated with SNAP was tested and is shown in Fig. 3**c**. Even without UC crystals, the NO release can be controlled if visible light directly irradiates a specimen. However, unlike the 980 nm light, white light does not penetrate through deep tissue (especially the green light absorbed by SNAP) and the use of white light to release NO is, therefore, not realistic for in-vivo applications.

The scaffolds were immersed in SBF for up to 2 weeks. The pH of the SBF solutions increases overtime due to the leaching of alkaline and alkaline earth ions and Na^+/H^+ exchange as suggested in [6] (Fig. 4**a**). As expected, the scaffold mass loss increases confirming the progressive dissolution of the scaffold in SBF (Fig. 4**b**). As depicted in Fig. 4**c**, the investigated scaffolds release Si in SBF and consume P overtime confirming not only the dissolution of the scaffold in SBF but also the formation of CaP layer at the scaffold surface. Therefore, our in-vitro study suggests that despite the addition of the upconverter crystals in the scaffolds, they remain bioactive. As the amount of rare-earth ions represents less than 1 wt% of the total mass of the scaffold, we expect the newly developed biophotonic scaffolds to be safe. Moreover, despite the formation of the reactive layer at the scaffold surface, no changes in the intensity of the green and red emission within 10% error margin could be detected after 2 weeks in SBF. This indicates that SNAP-NO can be released in-situ and on demand for at least 2 weeks following implantation.

Preliminary cytocompatibility test was performed, using hADSCs, in direct contact with the scaffolds (with and without up-converter particles). The aim was to assess if the degradation of the UC particles may impact negatively the cells viability.

Fig. 5 presents the live/dead images, taken at the bottom of the well plate ("bottom") and at the scaffolds surface ("top"). The control ("Ctrl") are cells cultured in the well plate.

As shown in the control condition ("Ctrl") cells were proliferating in the culture well plate, as expected. It should be noted that, here, the control only aims at showing the proper cell viability and proliferation of the cell line used. Comparison between cell cultured in contact with the samples and the control cannot be made. Overall, cells cultured in contact with the samples (with and without UC) does not lead to cell death. Cells remain viable in both conditions until 7 days of culture, around and on the top of the scaffold. However, the proliferation appears slow. This is expected from [6]. Indeed, while B50 (discs and extracts) led to slow cell proliferation their osteogenic properties outperformed those of typical commercially available bioactive glass S53P4 [6]. Slow proliferation of the hADSCs, in contact with B50 glass or extract, was reported to be to 1) the high pH due to the fast glass dissolution and/or 2) the early differentiation of the cells known to disrupt the cell proliferation. The addition of UC to the B50 glass does not induce any significant change in cell viability, around and at on the top of the scaffolds.

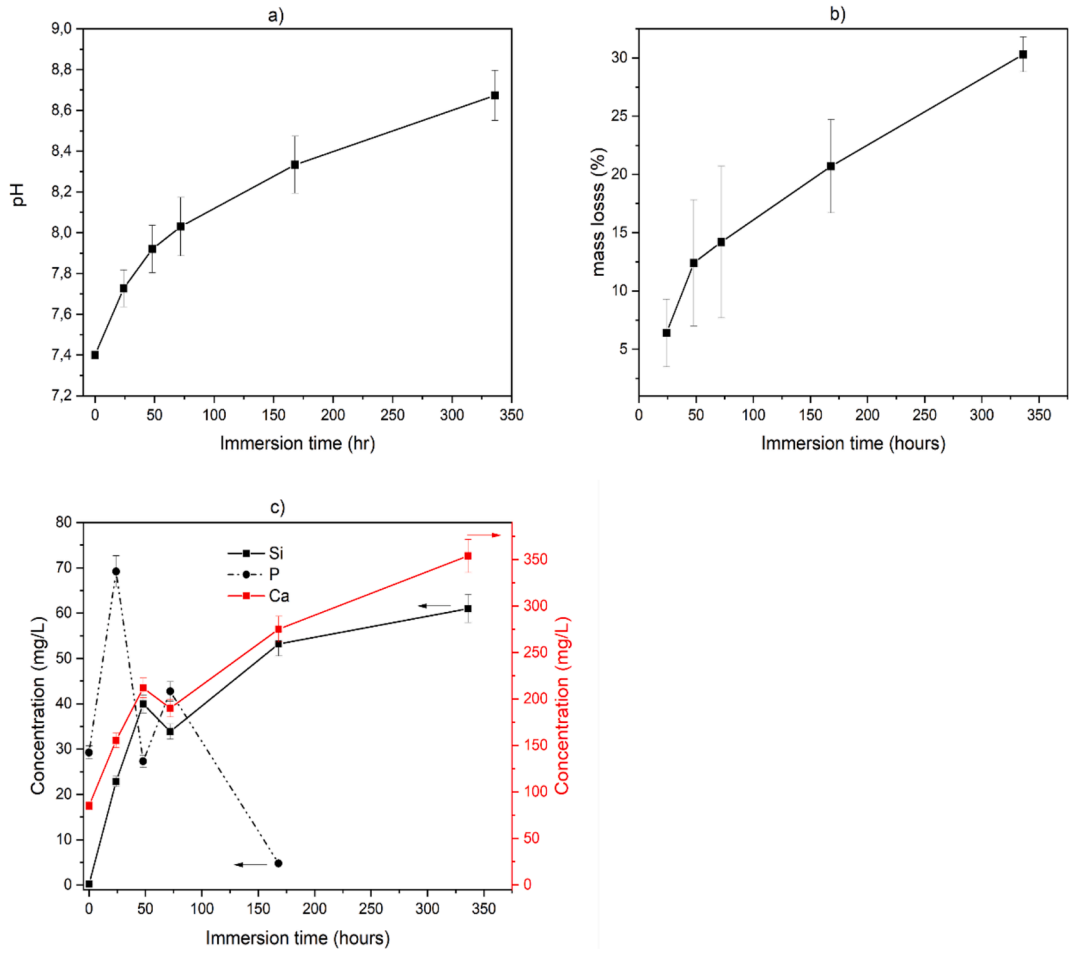

Fig. 4. Response of scaffold in time during SBF immersion: solution pH (a), scaffold percentage mass loss (b) and concentrations of P, Ca and Si in the immersion solution (c).

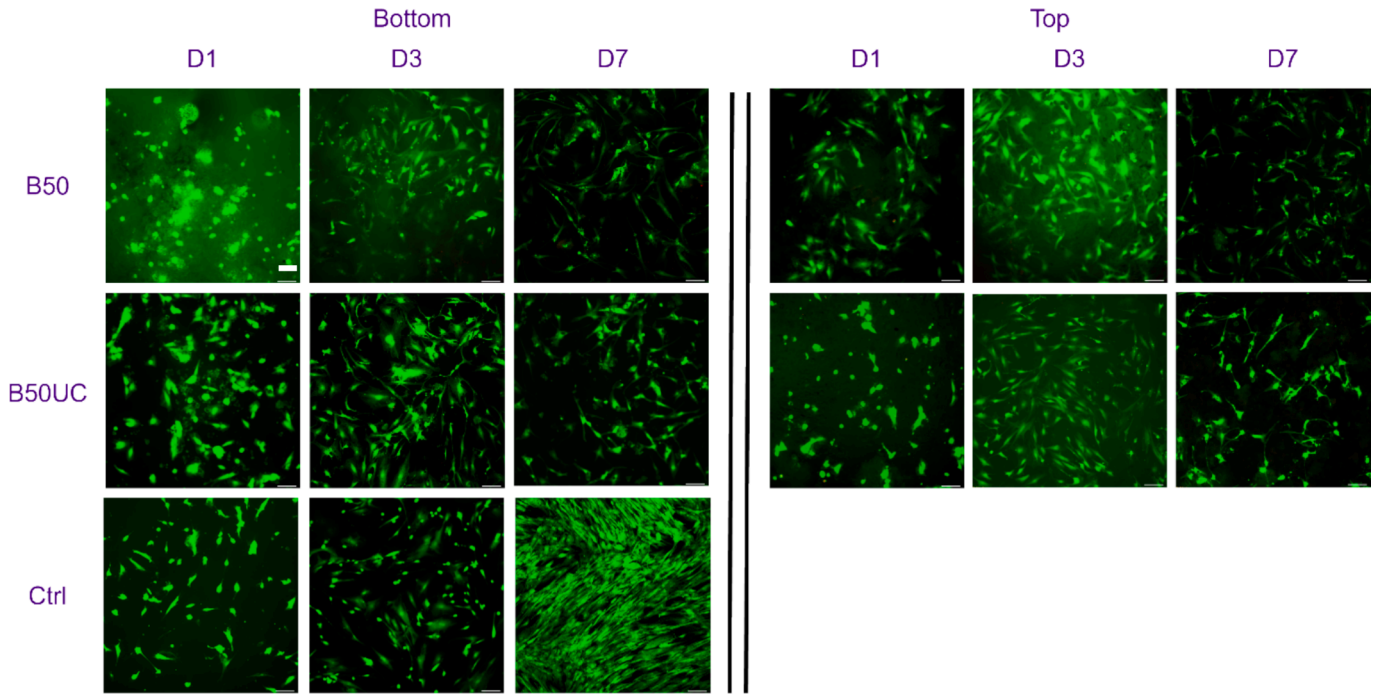

Fig. 5. Fluorescence microscopy images, showing human adipose stem cells viability, by Live/Dead assay, around ("bottom") and at the surface ("Top") of bioactive glass scaffold B50 and B50UC. Ctrl represents cells cultured on a well plate without samples. Scale bar: 200 μm.

4. Conclusion

In summary, we demonstrated that Er^{3+}, Yb^{3+} co-doped $CaWO_4$ crystals can be added in borosilicate glass prior to sintering to obtain porous scaffolds using the porogen technique with target porosity ((68 ± 2.5) %), Young's modulus ((37 ± 15) MPa) and maximum compressive strength ((0.9 ± 0.3) MPa). The scaffolds emit a brightness measured at 2.3cd/m^2 under 3 mW/cm^2 power density using 980 nm laser diode, which is enough to release NO from SNAP covered scaffolds in controlled manner. The addition of the crystals, up to 10 wt%, has no significant impact on the bioresponse of the scaffold. Green light could still be seen from the scaffolds under 980 nm pumping after 2 weeks on immersion in SBF suggesting that NO could be released using 980 nm for at least 2 weeks after implantation and opens the path to light modulated active agent release.

Our study clearly shows the potential of the newly developed upconverter and bioactive scaffold for NO release under 980 nm pumping. The presence of Yb^{3+} and Er^{3+}, and the slow degradation of the UC particles does not impact the cell viability and all prepared materials appears cytocompatible.

CRediT authorship contribution statement

S. Ghanavati: Writing – review & editing, Writing – original draft, Methodology, Investigation, Formal analysis, Data curation, Conceptualization. **E. Santos Magalhaes:** Writing – review & editing, Writing – original draft, Validation, Methodology, Investigation, Formal analysis, Data curation. **C. Nguyen:** Writing – review & editing, Writing – original draft, Methodology, Formal analysis, Data curation. **B. Bondzior:** Writing – review & editing, Writing – original draft, Methodology, Investigation, Formal analysis, Data curation. **M. Lastusaari:** Writing – review & editing, Writing – original draft, Validation, Supervision, Methodology, Investigation, Formal analysis, Data curation. **J.N. Anker:** Writing – review & editing, Writing – original draft, Validation, Methodology, Formal analysis, Conceptualization. **A. Draganski:** Writing – review & editing, Writing – original draft, Visualization, Methodology, Investigation, Formal analysis, Data curation, Conceptualization. **L. Petit:** Writing – review & editing, Writing – original draft, Validation, Supervision, Resources, Project administration, Methodology, Investigation, Funding acquisition, Formal analysis, Data curation, Conceptualization. **J. Massera:** Writing – review & editing, Writing – original draft, Validation, Supervision, Resources, Project administration, Methodology, Investigation, Funding acquisition, Formal analysis, Data curation, Conceptualization.

Declaration of competing interest

The authors declare the following financial interests/personal relationships which may be considered as potential competing interests: L. Petit reports financial support was provided by Research Council of Finland. J. Massera reports financial support was provided by Research Council of Finland. If there are other authors, they declare that they have no known competing financial interests or personal relationships that could have appeared to influence the work reported in this paper.

Acknowledgements

This work was supported by Academy of Finland [Flagship Programme, Photonics Rese arch and Innovation PREIN-320165] and Academy Projects -328077 and 331924. The graphical abstract was produced using Biorender.com.

Data availability

Data will be made available on request.

References

[1] E. Axinte, Glasses as engineering materials. A review, Mater. Des. 32 (4) (2011) 1717–1732.
[2] L.L. Hench, The story of bioglass, J. Mater. Sci. Mater. Med. 17 (11) (2006) 967–978.
[3] D. Zhang, E. Vedel, L. Hupa, H. Aro, Predicting physical and chemical properties of bioactive glasses from chemical composition. Part 3. In Vitro Reactivity, Glass Technol. 50 (1) (2009) 1–8.
[4] N.A.P. Van Gestel, J. Geurts, D.J.W. Hulsen, B. van Rietbergen, S. Hofmann, J. J. Arts, Clinical applications of S53P4 bioactive glass in bone healing and osteomyelitic treatment: a literature review, Biomed. Res. Int. 2015 (2015) 684826.
[5] M.N. Rahaman, D.E. Day, B.S. Bal, Q. Fu, S.B. Jung, L.F. Bonewald, A.P. Tomsia, Bioactive glass in tissue engineering, Acta Biomater. 7 (2011) 2355–2373.
[6] M. Ojansivu, A. Mishra, S. Vanhatupa, M. Juntunen, A. Larionova, J. Massera, S. Miettinen, The effect of S53P4-based borosilicate glasses and glass dissolution products on the osteogenic commitment of human adipose stem cells, PLoS One 13 (8) (2018) e0202740.
[7] E.P. Erasmus, R. Sule, O.T. Johnson, J. Massera, I. Sigalas, In vitro evaluation of porous borosilicate, borophosphate and phosphate bioactive glasses scaffolds fabricated using foaming agent for bone regeneration, Sci. Rep. 8 (1) (2018) 3699.
[8] C. Soundrapandian, S. Datta, B. Kundu, D. Basu, B. Sa, Porous bioactive glass scaffolds for local drug delivery in osteomyelitis: development and in vitro characterization, AAPS PharmSciTech 11 (2010) 1675–1683.
[9] World Health Organization, Antimicrobial resistance surveillance in Europe 2022–2020 data (2022).
[10] S.P. Hopkins, M.C. Frost, Synthesis and characterization of controlled nitric oxide release from S-nitroso-N-acetyl-d-penicillamine covalently linked to polyvinyl chloride (SNAP-PVC), Bioeng. 5 (3) (2018) 72.
[11] G.M. Buga, M.E. Gold, K.S. Wood, G. Chaudhuri, L.J. Ignarro, Endothelium-derived nitric oxide relaxes nonvascular smooth muscle, Eur. J. Pharmacol. 161 (1) (1989) 61–72.
[12] S.A. de Oliveira, R. Borges, D. dos Santos Rosa, A.C.S. de Souza, A.B. Seabra, F. Baino, J. Marchi, Strategies for cancer treatment based on photonic nanomedicine, Materials 14 (2021) 1435.
[13] J.L. Sandell, T.C. Zhu, A review of in-vivo optical properties of human tissues and its impact on PDT, J. Biophotonics 4 (11–12) (2011) 773–787.
[14] F. Auzel, Upconversion processes in coupled ion systems, J. Lumin. 45 (1990) 341–345.
[15] J. Ye, J. Jiang, Z. Zhou, Z. Weng, Y. Xu, L. Liu, W. Zhang, Y. Yang, J. Luo, X. Wang, Near-infrared light and upconversion nanoparticle defined nitric oxide-based osteoporosis targeting therapy, ACS Nano 15 (2021) 13692–13702.
[16] X. Li, Q. Zou, J. Wie, W. Li, The degradation regulation of 3D printed scaffolds for promotion of osteogenesis and in vivo tracking, Compos. B 222 (2021) 109084.
[17] M.J. Treadaway, R.C. Powell, Luminescence of calcium tungstate crystals, J. Chem. Phys. 61 (1974) 4003–4011.
[18] R.M. Hazen, L.W. Finger, J.W.E. Mariathasan, High-pressure crystal chemistry of scheelite-type tungstates and molybdates, J. Phys. Chem. Solids. 46 (2) (1985) 253–263.
[19] X. Wang, Y. Wang, Y. Bu, X. Yan, J. Wang, P. Cai, T.V.H.J. Seo, Influence of doping and excitation powers on optical thermometry in Yb3+- Er3+ doped CaWO4, Sci. Rep. 7 (1) (2017) 43383.
[20] M.M. Suckey, D.W. Benza, J.D. DesJardins, J.N. Anker, Upconversion spectral rulers for transcutaneous displacement measurements, Sensors 21 (10) (2021) 3554.
[21] E.B.W. Giesen, M. Ding, M. Dalstra, T.M.G.J. Van Eijden, Mechanical properties of cancellous bone in the human mandibular condyle are anisotropic, J. Biomeh. 34 (6) (2001) 799–803.
[22] E.J. Brisbois, H. Handa, T.C. Major, R.H. Barlett, M.E. Meyerhoff, Long-term nitric oxide release and elevated temperature stability with S-nitroso-N-acetylpenicillamine (SNAP)-doped Elast-eon E2As polymer, Biomater. 34 (28) (2013) 6957–6966.
[23] S.P. Hopkins, J. Pant, M.J. Goudie, H. Handa, Achieving long-term biocompatible silicone via covalently immobilized S-nitroso-N-acetylpenicillamine (SNAP) that exhibits 4 months of sustained nitric oxide release, ACS Appl. Mater. Interfaces. 10 (32) (2018) 27316–27325.
[24] E.P. Erasmus, O.T. Johnson, I. Sigalas, J. Massera, Effects of sintering temperature on crystallization and fabrication of porous bioactive glass scaffolds for bone regeneration, Sci. Rep. 7 (1) (2017) 6046.
[25] X. Cheng, C. Yuan, L. Su, Y. Wang, X. Zhu, Effects of pressure on the emission of CaWO4: Eu3+ phosphor, Opt. Mater. 37 (2014) 214–217.
[26] E. Santos Magalhaes, A. Sedda, B. Bondzior, S. Vuori, D. Van der Heggen, P. F. Smet, M. Lastusaari, L. Petit, Glass-based composites comprised of $CaWO_4$: Y^{b3} +, ^{Tm}3+ crystals and Sr_Al_2O4: ^{E}u2 +' Dy3+ phosphors for green afterglow after NIR charging, Ceram. Int. 49 (2023) 41150–41157.
[27] T. Kokubo, H. Takadama, How useful is SBF in predicting in vivo bone bioactivity, Biomaterials 27 (15) (2006) 2907–2915.
[28] P. Xie, S.C. Rand, Continuous-wave mode-locked visible upconversion laser, Opt. Lett. 17 (16) (1992) 1116–1118.
[29] W. Xu, X. Gao, L. Zheng, P. Wang, Z. Zhang, W. Cao, Optical thermometry through green upconversion emissions in Er3+/Yb3+- codoped $CaWO_4$ phosphor, Appl. Phys. Express. 5 (7) (2012) 072201.
[30] X. Luo, W. Cao, Blue, green, red upconversion luminescence and optical characteristics of rare earth doped rare earth oxide and oxysulfide, Sci. China, Ser. B: Chem. 50 (4) (2007) 505–513.

[31] E.P. Erasmus, R. Sule, O.T. Johnson, J. Massera, I. Sigalas, In vitro evaluation of porous borosilicate, borophosphate and phosphate bioactive glasses scaffolds fabricated using foaming agent for bone regeneration, Sci. Rep. 8 (2018) 3699.
[32] M. Fabert, N. Ojha, E. Erasmus, M. Hannula, M. Hokka, J. Hyttinen, J. Rocherullé, I. Sigalas, J. Massera, Crystallization and sintering of borosilicate bioactive glasses for application in tissue engineering, J. Mater. Chem. B 5 (2017) 4514–4525.
[33] Q. Fu, E. Saiz, M.N. Rahaman, A.P. Tomsia, Bioactive glass scaffolds for bone tissue engineering: state of the art and future perspectives, Mater. Sci. Eng. Mater Biol Appl. 31 (2012) 1245–1256.
[34] D. Yang, Q. Pan, S. Kang, G. Dong, J. Qiu, Weakening thermal quenching to enhance luminescence of Er3+ doped β-NaYF4 nanocrystals via acid-treatment, J. Am. Ceram. 102 (10) (2019) 6027–6037.
[35] N. Ojha, M. Bogdan, R. Galatus, L. Petit, Effect of heat-treatment on the upconversion of NaYF4: Yb3+, Er3+ nanocrystals containing silver phosphate glass, J. Non Cryst. Solids 544 (2020) 120243.